Electronic structures of silver oxides

Jeremy P. Allen,[*] David O. Scanlon, and Graeme W. Watson[†]

School of Chemistry and CRANN, Trinity College Dublin, Dublin 2, Ireland

The oxides of silver have a number of important technological applications, including use in battery technology, catalysis, and in the treatment of dermatological conditions. However, only the Ag_2O phase has been well characterized in previous work. To this end, this paper characterizes the electronic structures of the major oxide forms, namely, Ag_2O, Ag_2O_3, and AgO, using standard density functional theory (DFT), Hartree-Fock, and hybrid-DFT approaches. The optical properties are also assessed for these materials, enabling comparisons to be drawn to experiment and the origin of optical band gaps to be explained. The calculated optical gaps also suggest that electrodeposited Ag_2O films may not consist of pure material. Hartree-Fock calculations are seen to fail to model Ag(I) species correctly, due to the neglect of correlation. DFT and hybrid-DFT methods are seen to perform better, but problems due to the lack of van der Waals interactions are identified. Preliminary calculations using empirical dispersion corrections are discussed.

PACS number(s): 71.20.−b, 71.20.Nr, 71.15.Mb

I. INTRODUCTION

The oxides of silver are known to exhibit both Ag(I) and Ag(III) oxidation states, giving rise to a number of different phases. The range of different oxide stoichiometries differentiates it from the related copper-oxygen and gold-oxygen systems, which are much more restricted. Binary oxides of copper exist in the form of Cu_2O, CuO,[1] and the mixed valence Cu_4O_3.[2] For gold, however, only the Au(III) oxide is known, Au_2O_3,[3] although Au_2O has been suggested as a possible intermediate in its thermal decomposition.[4] In the silver-oxygen system, monovalent Ag(I) (Ag_2O) (Ref. [5]) and trivalent Ag(III) (Ag_2O_3) (Refs. [6–8]) binary oxides are known but there is no divalent Ag(II) oxide. Mixed valence oxides have also been reported, namely, Ag(I,III), AgO,[9] and the metallic Ag(II,III), Ag_3O_4.[10–13] In addition, evidence also exists for Ag_4O_3, through the electrochemical reduction of AgO,[14] and Ag_6O_2, which possesses $(Ag_6)^{4+}$ clusters.[15]

The oxides of silver have a number of important applications. Both Ag_2O and AgO have uses in battery technologies[16–19] and antibacterial applications.[20–22] Ag_2O is also used in molecular sensor technologies,[23] for example, as an enzymeless glucose sensor with Cu,[23,24] water splitting,[25] optical memories,[26] and organic catalysis, for example, in transmetalation[27] and the oxidation of aldehydes by molecular oxygen.[28] Additionally, Ag_2O is used as a component of a range of fast-ion conducting glasses of the form AgI-Ag_2O-MoO_3,[29] AgI-Ag_2O-WO_3,[30] AgI-Ag_2O-V_2O_5,[31] and AgI-Ag_2O-P_2O_5.[32]

Ag_2O has been the most widely studied of the different silver oxides, with investigations mainly focusing on the electronic structure of the material[33–36] and the interaction and bonding between the silver and oxygen atoms (primarily concerning the degree of covalency).[33,37,38] The closed shell d^{10} nature of Ag(I) may be thought to give rise to a purely ionic system, however, calculations by Czyżyk et al.[34] and Deb and Chatterjee[33] have shown that the valence band of Ag_2O consists mainly of O 2p and Ag 4d states with a significant, albeit small, contribution from Ag 5s states. X-ray photoelectron spectroscopy (XPS), and Auger-electron and bremsstrahlung isochromat spectroscopy (BIS) studies

by Tjeng et al.[35] report a fundamental band gap of 1.3 eV. Calculated band gaps using standard density functional theory (DFT) methods are typically underestimated, with reported values of 0.40 (Ref. [34]) and 0.08 eV,[39] or the material is predicted to be metallic.[33] The experimental optical band gap, obtained from absorption spectra of Ag_2O thin films, is reported to be 2.25 eV.[40] More recent experimental studies on nanoparticles[41] and electrodeposited thin films,[42] however, have placed the optical band gap at 1.46 eV.

Ag_2O_3 has had considerably less attention in the literature than Ag_2O, most likely due to its poor stability. Studies of Ag_2O_3 have either detailed the crystal structure[6–8] or used x-ray absorption near-edge spectroscopy (XANES) and [109]Ag magic angle spinning (MAS) NMR to characterize Ag(III) ions. In XANES, Ag(III) shows a higher-energy L_1 peak and a more intense L_3 peak than Ag(I) species due to a lower occupation of the d shell.[43] The [109]Ag MAS NMR study of van Wüllen et al. showed that Ag(III) ions have a higher chemical shift in NMR spectra than Ag(I) ions.[44] Using DFT, Burdett and Sevov[45] previously calculated a density of states for Ag_2O_3, along with other group 11 sesquioxides, finding a band gap of 0.96 eV and mixing of the O 2p and Ag 4d states in the valence band.

Although AgO has also been studied to a lesser extent than Ag_2O, a number of investigations have attempted to elucidate the exact oxidation states present. XANES,[43] [109]Ag MAS NMR,[44] and x-ray absorption spectroscopy[46] studies have identified the material as containing both Ag(I) and Ag(III) valences. XPS data,[36,46,47] however, has led to some controversy through the observation of two peaks for O 1s, suggesting two oxidation states for O. Bielmann et al.[47] attributed this to AgO possessing a mixed (I,II) oxidation state with hole states present on the O anions, based on early theoretical studies by Park et al.[48] However, the second peak was explained by Hoflund et al.[36] to be a result of Ag_2CO_3 impurities, which are present due to it having a greater thermal stability than AgO and therefore it is very difficult to remove. Furthermore, we previously used a hybrid-DFT methodology to show that AgO exists with Ag(I) and Ag(III) oxidation states, and that standard DFT methods are unable to capture

this mixed valence nature, predicting a symmetric Ag(II)O structure.[49]

This paper examines the electronic structure and bonding properties of Ag_2O, Ag_2O_3, and AgO through the characterization of the densities of states and band structures using standard DFT, Hartree-Fock, and hybrid-DFT methodologies. This will provide a comprehensive and comparative analysis of these common silver oxides, allowing a full understanding of the structure and bonding in the silver-oxygen system.

II. COMPUTATIONAL METHODS

All calculations in this paper are performed using the periodic DFT code VASP.[50,51] This uses a plane-wave basis set to describe the valence electronic states, with interactions between the cores (Ag:[Kr] and O:[He]) and the valence electrons described using the projector-augmented wave[52,53] (PAW) method. This paper uses three functionals for simulating the silver oxide structures. The first is the generalized gradient approximation (GGA) of Perdew, Burke, and Ernzerhof[54] (PBE) functional. The second uses the hybrid-DFT approach of Heyd, Scuseria, and Ernzerhof (HSE06).[55,56] The HSE06 method is a screened hybrid-DFT approach, in which a percentage of the PBE exchange is replaced with exact nonlocal Fock exchange. The HSE06 methodology, as described in more detail elsewhere,[55–57] uses a screening of $\omega = 0.11$ bohr^{-1} to partition the exchange into long- and short-range parts, where 25% of the PBE exchange in the short-range component is replaced with exact Fock exchange. Hybrid methods are more computationally demanding than the PBE functional; however, they are often found to give improved data for semiconductor systems, including atomic and electronic structure (including band gaps),[58–61] optical transitions,[62–64] and defective[65–67] and magnetic[68–70] systems. The third approach is the use of Hartree-Fock (HF), 100% exchange and no correlation, to assess the role of correlation and full exchange. The accurate prediction of the band gap from a band structure is only possible using a quasiparticle approach, for example, the GW method. However, HSE06 has been shown to afford reasonable values of direct and indirect fundamental gaps in comparison to experiment, and therefore the band gaps determined in this paper can be accepted with a reasonable level of confidence.[59,71]

The failure of DFT to model the mixed valence nature of AgO (Ref. 49) most likely results from the self-interaction error present in DFT, which favors the delocalization of highly correlated electrons. Although HSE06 is one approach to help correct this error, an alternative is the $GGA + U$ approach. This approach, which is less computationally demanding than HSE06, adds a correction, defined by the $+U$ term, to specific orbitals and acts as a penalty to the delocalization of electrons. The $GGA + U$ method has been previously shown to accurately describe polaronic n-type[72–76] and p-type[77,78] systems. Furthermore, $GGA + U$ has also been of use to predict the correct mixed valence in reduced ceria, namely, Ce(III) and Ce(IV) ions, which GGA fails to accurately model.[73,75] This method should therefore penalize against the formation of the equivalent Ag(II) ions, thus allowing the correct mixed valence of Ag(I,III) to be reproduced. Both the value of the U term and its ability to localize the d electrons will be assessed

through the application of the rotationally invariant form of $DFT + U$.[79] As Ag_2O and Ag_2O_3 do not have mixed oxidation states, this method is only used for modeling AgO.

Equilibrium lattice parameters for the bulk systems were determined through a series of structural minimizations at different volumes. In each calculation, the atomic coordinates, lattice vectors, and angles were allowed to fully relax within the constraint of a fixed total cell volume. The resultant energy-volume curves were then fitted to the Murnaghan equation of state to obtain the equilibrium bulk cell volume.[80] This approach avoids potential problems of Pulay stress and changes in the basis set which can accompany volume changes in plane-wave calculations. A plane-wave cutoff of 400 eV was used for all calculations and k-point grids of $4 \times 4 \times 4$, $4 \times 4 \times 6$, and $4 \times 6 \times 4$ were used for Ag_2O, Ag_2O_3, and AgO, respectively, where Ag_2O_3 was modeled in its primitive unit cell. For each calculation, structural minimization was deemed complete when the forces on all atoms were less than 0.01 eV Å^{-1}.

The optical absorption spectra, as well as the optical transition matrices, were calculated within the transversal approximation,[81] as described by Scanlon *et al.*[57] This approach sums all direct valence-band (VB) to conduction-band (CB) transitions on k-point grids to determine the optical absorption and does not include indirect and intraband transitions.[82] As only single-particle transitions are included, any electron-hole correlations would require higher-order electronic structure methods.[83,84] However, this approach has been shown to provide reasonable optical absorption spectra in comparison to experiment.[63,85–87]

III. RESULTS

A. Silver (I) oxide, Ag_2O

Ag_2O is isostructural with Cu_2O (Ref. 88) and crystallizes in the cubic $Pn\bar{3}m$ space group, with a lattice vector of 4.73 Å.[5] The unit cell [Fig. 1(a)] is highly symmetric and contains two interpenetrating cristobalite sublattices. The Ag(I) atoms are linearly coordinated to oxygen atoms, as expected for a d^{10} species,[89] whereas the oxygen atoms are tetrahedrally coordinated to the Ag(I) atoms, as detailed in Fig. 1(b). All bond distances within the system are equivalent, with Ag-O and nearest-neighbor Ag-Ag distances of 2.05 and 3.35 Å, respectively. Table I details the lattice vector and bond distances, with percentage differences to experiment, following structural minimization with the GGA, HSE06, and HF methods. The best reproduction of the experimental structure is seen with the hybrid-DFT functional, with a 2.0% difference to experiment, compared to 2.4% for GGA and 5.9% for HF. The HF approach is seen to give a significantly expanded lattice, relative to experiment, and the percentage errors seen for the GGA and HSE06 methods are also slightly larger than would normally be expected,[57,63,90,91] which will be discussed in Sec. IV.

The band structure calculated with the GGA and HSE06 functionals along the space-group high-symmetry lines from Bradley and Cracknell[92] are given in Fig. 2. Both methods give rise to a similar basic structure, which is also in broad agreement with previous calculations.[33,34,38,39] However, the
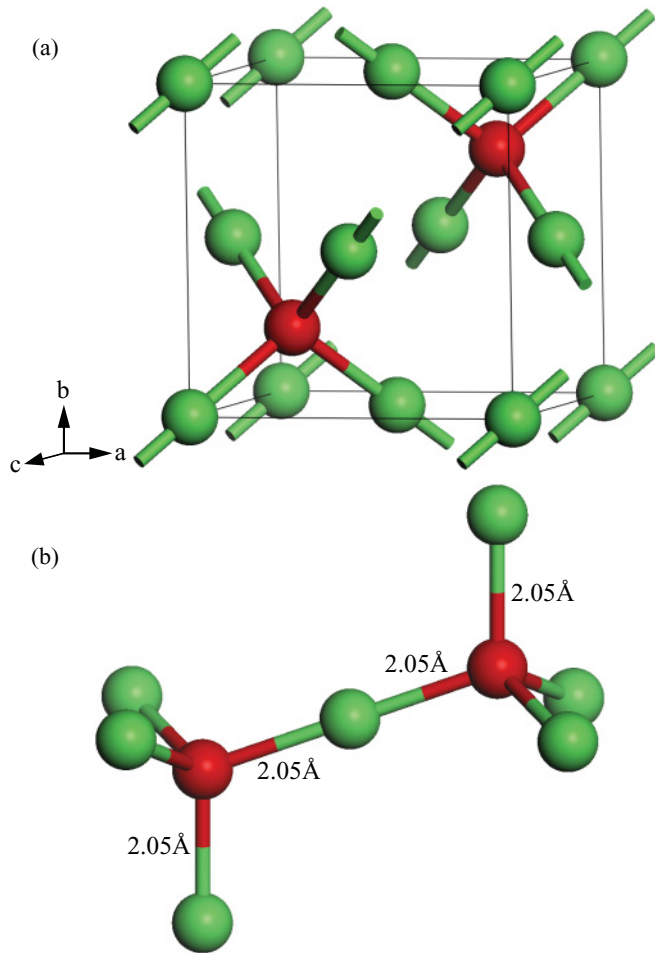
FIG. 1. (Color online) Atomic structure of (a) the unit cell of Ag_2O and (b) the coordination environment of Ag(I) ions, with experimental bond lengths (Ref. 5). Silver (I) and oxygen atoms are colored green (light gray) and red (dark gray), respectively.

GGA functional fails to predict a band gap [Fig. 2(a)], giving rise to a metallic system through the overlap of the VB and CB at the Γ point, similar to that seen by Deb and Chatterjee.[33] This is greatly improved through the use of hybrid-DFT [Fig. 2(b)], where the CB is shifted up in energy, relative to the VB, opening up a band gap. In comparison to GGA, the HSE06 valence band is also slightly broadened, by 0.4 eV,

TABLE I. Experimental lattice vector and bond lengths for Ag_2O with those calculated using GGA, HSE06, and HF methods. Percentage changes to experiment are given in parentheses and all values are in Å, except for the cell volume, which has units of $Å^3$.

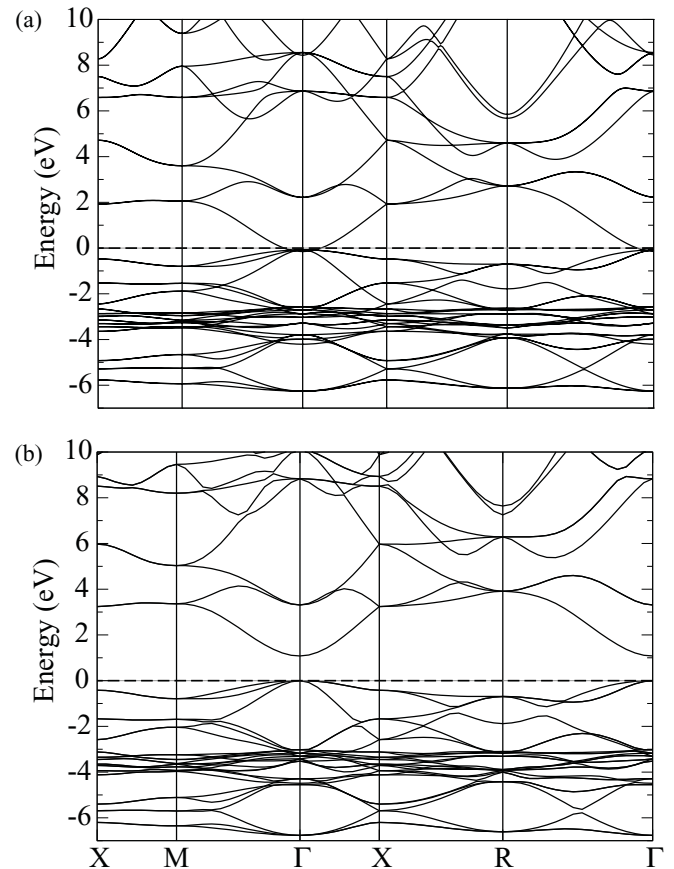| Property	GGA	HSE06	HF	Experiment (Ref. 5)
Lattice vector	4.844	4.824	5.012	4.731
	(2.4)	(2.0)	(5.9)	
Volume	113.64	112.27	125.90	105.86
	(7.1)	(5.8)	(18.9)	
Ag-O	2.097	2.089	2.170	2.048
	(2.4)	(2.0)	(6.0)	
Ag-Ag	3.425	3.411	3.544	3.345
	(2.4)	(2.0)	(5.9)	

FIG. 2. Calculated band structure for Ag_2O using the (a) GGA and (b) HSE06 functional. The top of the valence band in set to 0 eV, or, in the case of the GGA functional, the Fermi energy.

to a value of 6.8 eV, which is in better agreement with XPS data ($\sim$7 eV).[35] Both the valence-band maximum (VBM) and conduction-band minimum (CBM) are located at the Γ point, giving a direct fundamental band gap of 1.1 eV. This compares favorably with the XPS and BIS experimental fundamental band gap of 1.3 eV.[35] HSE06 was also seen to provide a band gap which was in very good agreement with experiment for isostructural Cu_2O.[93] The HF-calculated band structure (not shown) is also qualitatively similar to those determined with GGA and HSE06. However, the direct fundamental band gap is considerably overestimated, with a value of 8.30 eV at the Γ point. This overestimation is unsurprising as HF methods are well known to predict unoccupied states which are too high in energy.[94]

The calculated total and partial (ion and l-quantum number decomposed) electronic densities of states (EDOS and PE-DOS, respectively) using hybrid-DFT are shown for Ag_2O in Fig. 3. The EDOS, dominated by the Ag 4d and O 2p states, can be broadly separated into five regions, with the valence band comprising regions I–IV and region V representing the conduction band. Region I is primarily made up of O 2p states, with some mixing of Ag 4d states. The lower limit of this region also includes a small amount of Ag 5s states. Region II contains the majority of the Ag 4d states with only a minor contribution from O 2p. Region III is similar to region I in that it comprises mixed Ag 4d and O 2p states. Region IV makes
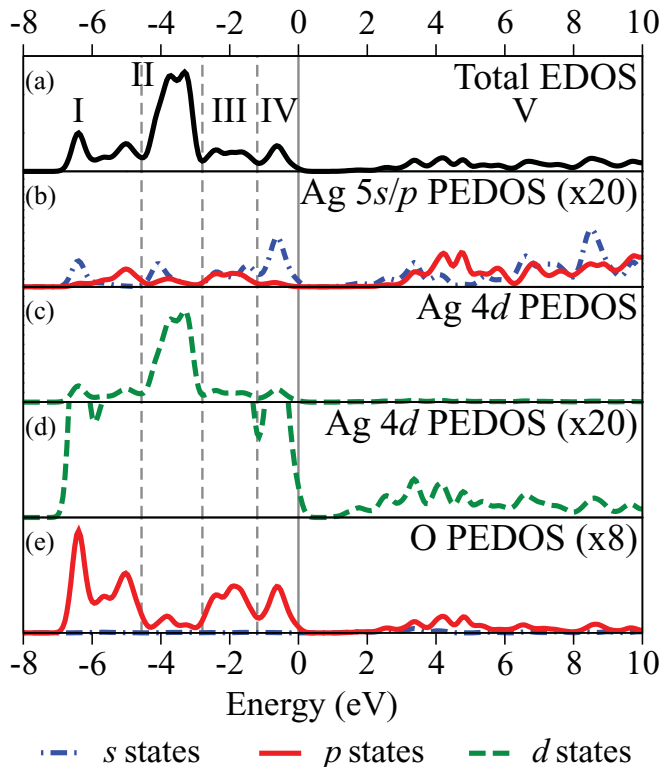
FIG. 3. (Color online) HSE06-calculated electronic density of states for Ag_2O. (a) Total EDOS, (b) Ag 5s and 5p PEDOS, (c) Ag 4d PEDOS, (d) Ag 4d PEDOS (multiplied to show the CB features), and (e) O PEDOS. The s, p, and d states are colored blue (dashed-dotted), red (dashed), and green (solid), respectively. The Fermi energy is represented by the vertical solid gray line, which has been set to 0 eV.
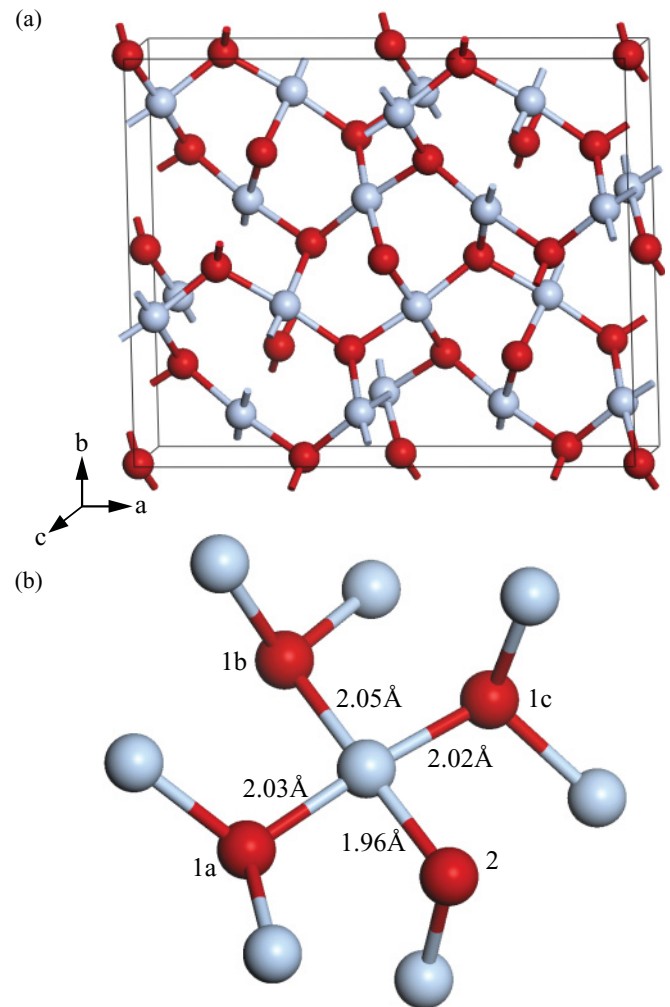

FIG. 4. (Color online) Atomic structure of (a) the unit cell of Ag_2O_3 and (b) the coordination environment around a silver atom, with bond distances from the experimental structure (Ref. 7). Silver (III) atoms are colored light blue (light gray) and oxygen atoms are colored red (dark gray).

up the VBM and is similar in character to the lower section of region I. It is mainly a mix of Ag 4d and O 2p states, with a Ag 5s contribution. The bottom of the conduction band, region V, consists primarily of Ag 5s, p and 4d states, with the d states having a stronger presence. The general appearance and features of the EDOS and PEDOS are consistent with previous studies.[34,35,38,39,95] The HSE06 results are seen to be superior to those of GGA, again shown by the valence band width and the increased band gap. The density of states calculated using the GGA and HF methods are seen to be similar in appearance to the HSE06 method, albeit with reduced and enlarged band gaps, respectively, and are therefore not shown.

The observation of Ag 5s states at the VBM and Ag 4d states at the CBM are indicative of a partial deoccupation of d states through s-d hybridization, rather than a d^{10} Ag species. This partial deoccupation has also been reported in experimental Ag L_3 XANES spectra[43] and computational studies.[34,38,39,95] A similar bonding scheme with s-d hybridization has also been observed previously for Cu_2O.[96]

B. Silver (III) oxide, Ag₂O₃

Ag_2O_3 possesses an orthorhombic structure (space group $Fdd2$),[7] shown in Fig. 4(a), and is isostructural with Au_2O_3.[97] The structure comprises slightly distorted AgO_4 subunits, with the d^8 Ag(III) ions possessing an approximate square planar coordination to four oxygen atoms [Fig. 4(b)], as expected

due to crystal-field effects.[89] Three of the oxygen atoms are bonded to three silver atoms, labeled O_{1a}, O_{1b}, and O_{1c}. The fourth oxygen atom, labeled O_2, is bound to only two silver atoms, giving rise to the slight distortion of the square planar environment. The calculated lattice vectors and bond lengths, along with experimental values,[7] are given in Table II. The HSE06 method is seen to perform noticeably better than GGA, reproducing the lattice constants to within 2.8% and the bond lengths to within 0.7%. HF gives an even better reproduction of lattice vectors, being within 1.6%, although the bond lengths are mainly underestimated, with some being up to 2.1% too small. All three methods show an expansion in the c vector, relative to the a and b vectors, which is not reflected in the predicted Ag-O bond lengths and is larger than typically seen for GGA/HSE06/HF calculations. From the structure, the c vector appears to be influenced by Ag-Ag interactions in particular, rather than an Ag-O bond, and therefore this interaction may give rise to the unexpected expansion. This will be further discussed in Sec. IV.

TABLE II. Experimental lattice vectors and bond lengths for Ag_2O_3 with those calculated using GGA, HSE06, and HF methods. Percentage changes to experiment are given in parentheses and all values are in Å, except for the cell volume, which has units of Å^3.

Property	GGA	HSE06	HF	Experiment (Ref. 7)
a	13.096	12.964	12.930	12.869
	(1.8)	(0.7)	(0.5)	
b	10.697	10.609	10.610	10.490
	(2.0)	(1.1)	(0.8)	
c	3.834	3.767	3.722	3.664
	(4.6)	(2.8)	(1.6)	
Volume	537.05	518.06	510.61	494.12
	(8.7)	(4.8)	(3.3)	
Ag-O_{1a}	2.077	2.037	2.011	2.029
	(2.4)	(0.4)	(−0.9)	
Ag-O_{1b}	2.089	2.060	2.044	2.046
	(2.1)	(0.7)	(−0.1)	
Ag-O_{1c}	2.056	2.014	1.980	2.021
	(1.7)	(−0.4)	(−2.0)	
Ag-O_2	1.999	1.958	1.919	1.961
	(1.9)	(−0.2)	(−2.1)	

The band structures calculated with the GGA and HSE06 functionals are given in Fig. 5. In comparison to GGA, the effect of the hybrid-DFT method can be seen to shift the CB up in energy relative to the VB, increasing the band gap. The valence band is also seen to be broadened slightly in the HSE06 calculation, relative to the GGA method. Although the two band structures are similar in structure, the location of the VBM is different. For the GGA-calculated band structure [Fig. 5(a)], the VBM is seen on the line between L and Γ. However, for HSE06 [Fig. 5(b)], the VBM is seen to occur in two locations, one between Γ-Z and the other between X and Y. The CBMs for GGA and HSE06 are both located between Z and L, giving indirect band gaps of 0.5 and 1.9 eV for the two methods, respectively. The smallest direct band gaps for GGA and HSE06 are 0.6 and 2.0 eV, respectively, located along the Z-L line in both cases. The band structure calculated using HF (not shown) is very similar in structure to those determined using GGA and HSE06. As with the HSE06 band structure, the HF VBM is found along the X-Y line but the CBM is seen to differ. The CBM with HF is instead found along the X-Y line, at a different position to the VBM, giving an indirect band gap. The band gaps are significantly overestimated, as expected, with values of 10.29 and 10.30 eV for the indirect and direct fundamental band gaps. The only previously calculated band gap is from the DFT study of Burdett and Sevov.[45] From their calculated EDOS, the band gap is estimated to be 0.96 eV, which is similar to our GGA value, albeit slightly higher due to their use of a different functional (the local density approximation).

The EDOS and PEDOS are shown for Ag_2O_3 in Fig. 6. with Ag_2O, the valence band is dominated by Ag 4d and O 2p states. The valence band can be split into three regions. Region I is seen to be mixed Ag 4d and O 2p (predominantly O_1) states, with a minor contribution from the Ag 5s states. The Ag 4d states increase in dominance through region II, reaching a maximum near to the boundary with region III. The
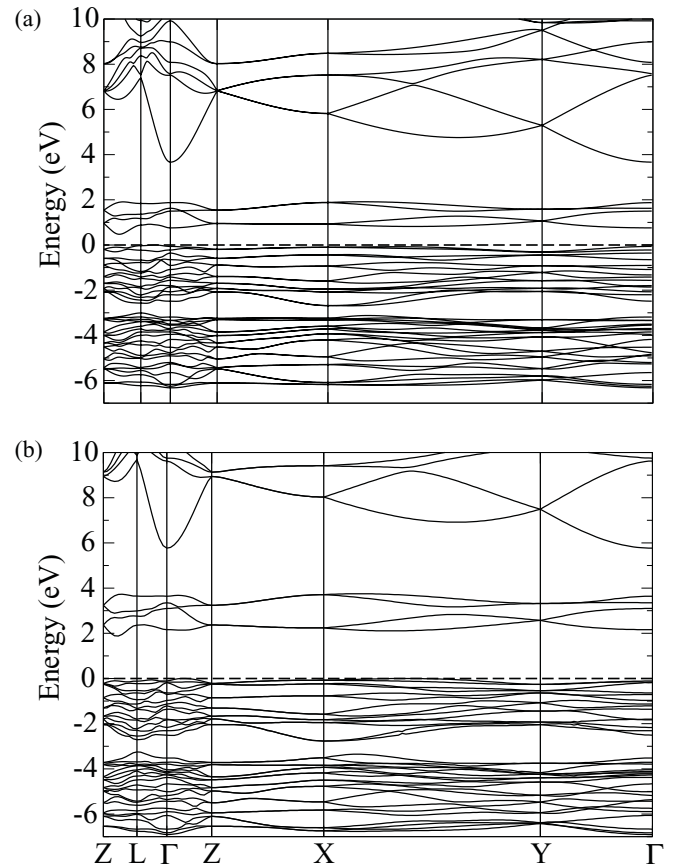

FIG. 5. Calculated band structure for Ag_2O_3 using the (a) GGA and (b) HSE06 functional. The top of the valence band in set to 0 eV.

opposite is true for the O_1 2p states, which can be seen to diminish throughout the region. Region III comprises the top of the VB and, as region I, is mainly composed of mixed Ag 4d and O 2p states, with minor contributions from the Ag 5s and p. In comparison to Ag_2O, this Ag 5s and p contribution to the VBM occurs over a greater energy range. The O 2p states in region III differ for the two types of coordination. While the O_1 2p states are seen to be equally spread throughout the region, those from the O_2 2p are concentrated at higher energy, near to the VBM. The conduction band is split into two regions, IV and V. Region IV contains the empty Ag 4d states, which are mixed with O 2p states, and is then separated by a gap of 2.0 eV from region V, which consists of Ag 5s and p and O 2p states.

The calculated EDOS, as well as the PEDOS, is consistent with previous work, in terms of both general structure and relative peak positions.[45] It is also qualitatively similar to that calculated for the isostructural Au_2O_3.[97] As HSE06 was seen to perform better for Ag_2O, widening the VB and increasing the band gap to values in closer agreement to experiment, it is therefore also likely to give more accurate results for Ag_2O_3.

C. Silver (I,III) oxide, AgO

AgO is known to crystallize in both monoclinic[9] and tetragonal[98] forms, with the former being the most commonly found and studied. The monoclinic structure, space group
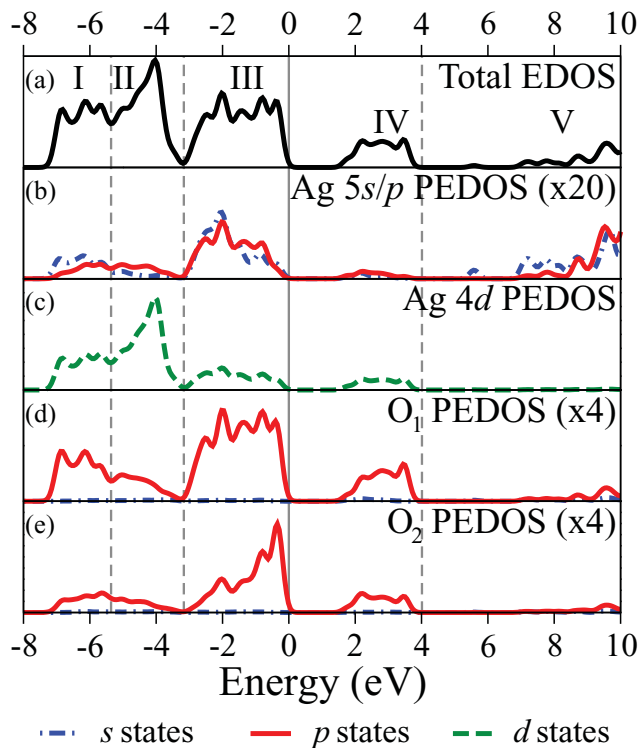
FIG. 6. (Color online) HSE06-calculated electronic density of states for Ag_2O_3. (a) Total EDOS, (b) Ag $5s$ and $5p$ PEDOS, (c) Ag $4d$ PEDOS, (d) O_1 PEDOS, and (e) O_2 PEDOS, where O_1 is a combination O_{1a}, O_{1b}, and O_{1c} states. The s, p, and d states are colored blue (dashed-dotted), red (dashed), and green (solid), respectively. The Fermi energy is represented by the vertical solid gray line, which has been set to 0 eV.
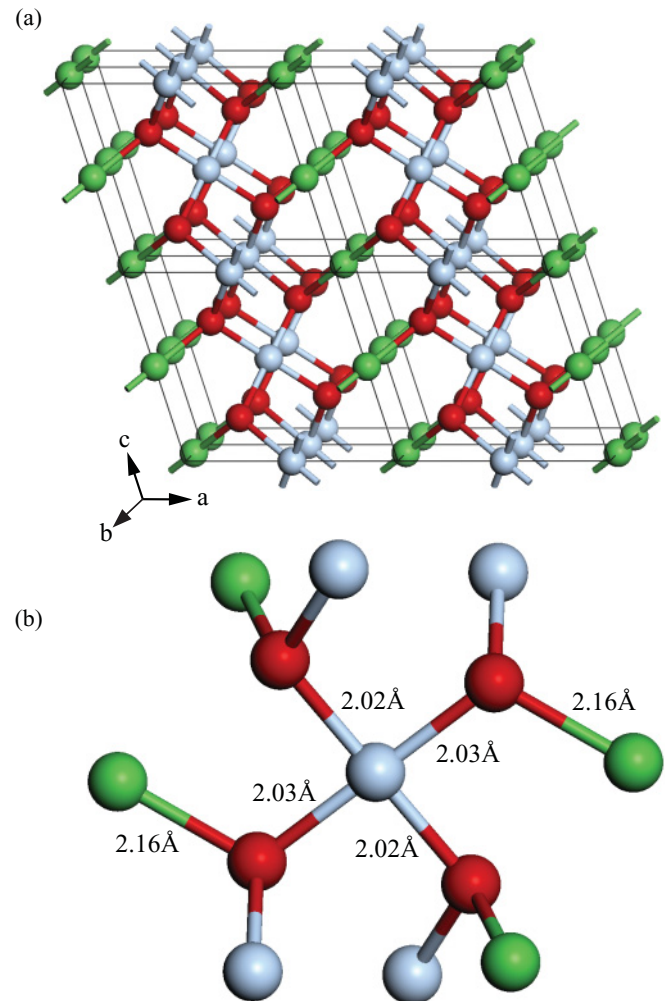

FIG. 7. (Color online) Atomic structure of (a) the unit cell of AgO, grown $2 \times 2 \times 2$ for clarity, and (b) the coordination environment around an Ag(III) ion, with corresponding bond lengths. Green (medium gray), light blue (light gray), and red (dark gray) spheres represent the Ag(I), Ag(III), and oxygen atoms, respectively. See text for details of bond angles around the Ag(III) ion.

$P12_1/c1$, possesses two different coordination environments, and associated oxidation states, for the silver ions, as shown in Fig. 7, which were previously shown to be Ag(I) and Ag(III) valences.[49] The Ag(I) ions have a linear coordination to oxygen with an Ag-O bond distance of 2.16 Å. The Ag(III) ions, however, have slightly distorted square planar environments, with bond distances of 2.02 and 2.03 Å, and bond angles of 88.6° and 91.4°. From a structural point of view, similarities can be seen between the structure of AgO with the corresponding Ag(I) and Ag(III) environments seen in Ag_2O and Ag_2O_3, Figs. 1 and 4, respectively. Although similar Ag(III)-O bond distances are seen in both AgO and Ag_2O_3, the Ag(I)-O bond distances are extended in AgO, compared to the 2.05 Å seen in Ag_2O.

Minimization of AgO was first conducted using the GGA, HSE06, and HF methods, with the optimized structural parameters and bond lengths provided in Table III. As we have previously reported,[49] the GGA and HSE06/HF methodologies predict different minimum energy structures. The HSE06 approach minimizes the structure to within reasonable agreement with experiment, with measured parameters varying from experiment by less than 3.3%. The HF method predicts the same structure as HSE06 but is a little more distorted, with errors in the lattice vectors of up to 5.8% greater than experiment. This distortion is seen to be caused by an overestimated Ag(I)-O bond length and underestimated Ag(III)-O

bonds. The GGA method, however, fails to capture the mixed valence character of this structure, with the minimized cell possessing equivalent silver atoms. The generated structure [Fig. 8(a)] shares similarities with the CuO structure, which formally possesses Cu(II) ions.[99] For comparison, Figs. 8(b) and 8(c) show the basic structural motif of a metal ion in the GGA-predicted AgO and experimental CuO structures, respectively. As can be seen, a similar bonding pattern is given by both materials, albeit with the AgO structure possessing a greater amount of symmetry in the square planar environment around the Ag ions. This is most likely due to the shorter Cu-O bond length causing more strain, which is alleviated by the distortion away from the symmetric coordination.

The probable cause of the failure of GGA is the self-interaction error that is present in standard DFT approaches, which favors the delocalization of charge giving rise to equivalent silver atoms. To assess the ability of the GGA + U approach to predict the correct Ag(I,III) mixed valence, we have applied U values ranging between 1 and 7 eV to

TABLE III. Experimental lattice vectors and bond lengths for AgO with those calculated using GGA GGA $+ U$, and HSE06 methods. For GGA $+ U$ calculations, where $U = 5$ or 6 eV, values for both Ag(II)O and Ag(I,III)O structure types are quoted. Percentage changes to experiment are given in parentheses and all values are in Å, except for the cell volume, which has units of Å^3.

Property	GGA	$U = 5$ eV		$U = 6$ eV		HSE06	HF	Experiment (Ref. 9)
		Ag(II)O	Ag(I,III)O	Ag(II)O	Ag(I,III)O			
a	4.738	4.777	5.718	4.804	5.727	5.934	5.957	5.859
	(-19.1)	(-18.5)	(-2.4)	(-18.0)	(-2.2)	(1.3)	(1.7)	
b	4.616	4.542	3.669	4.510	3.665	3.599	3.689	3.484
	(32.5)	(30.4)	(5.3)	(29.4)	(5.2)	(3.3)	(5.8)	
c	5.601	5.637	5.570	5.640	5.562	5.551	5.529	5.500
	(1.8)	(2.5)	(1.3)	(2.5)	(1.1)	(0.9)	(0.5)	
Volume	122.50	122.31	113.19	122.20	113.19	113.21	118.46	107.07
	(14.4)	(14.2)	(5.7)	(14.1)	(5.7)	(5.7)	(10.6)	
Ag(I)-O	2.167	2.168	2.224	2.168	2.242	2.155	2.311	2.161
	(0.3)	(0.3)	(2.9)	(0.3)	(3.7)	(-0.3)	(6.9)	
Ag(III)-O$_{short}$	2.167	2.168	2.069	2.168	2.066	2.015	1.985	2.023
	(7.1)	(7.2)	(2.3)	(7.2)	(2.1)	(-0.4)	(-1.9)	
Ag(III)-O$_{long}$	2.167	2.168	2.069	2.168	2.068	2.018	1.986	2.028
	(6.9)	(6.9)	(2.0)	(6.9)	(2.0)	(-0.5)	(-2.1)	

the Ag $4d$ states. Both the experimental [Ag(I/III)O] and GGA-predicted [Ag(II)O] structures were modeled with this method, calculating the predicted energy as a function of the unit cell volume, ranging between 103.89 and 131.17 Å^3. The energy-volume curves for these different approaches are provided in Fig. 9. No constraints other than allowing the lattice vectors and angles of the unit cell to vary under a constant total volume were applied to the systems. For all Ag(II)O simulations the structure was maintained. However, as the volume increases, a structural change from the Ag(I,III)O to the Ag(II)O unit cell was observed with the GGA $+ U$ method. Therefore, to give an estimate of the energy for the next volume, the unit-cell dimensions and angles were scaled and only the atomic coordinates were allowed to relax. These calculations are those termed "predicted energy for Ag(I,III)O structure" in Fig. 9 and are shown as open circles.

The GGA method is clearly seen to predict the erroneous Ag(II)O structure as being the lowest in energy at all modeled volumes. For the GGA $+ U$ method a number of observations can be identified. First, for a U value of 1 eV, it was not possible to obtain any energies for the Ag(I,III)O structure type as the structure always reverted to the Ag(II)O structure. Second, as the U value is increased, the energy of the Ag(I,III)O structure is stabilized, relative to the Ag(II)O structure, with a U value of 6 eV being the first to correctly predict the Ag(I,III)O structure as the lowest in energy. This suggests that the minimum value of U required to predict the correct ground-state electronic structure must, at least, be greater than 5 eV. Although this study simply considers the effect of U and does not attempt to determine an accurate value of U for this system, this is similar to that reported for Cu, where a U value of 5.2 eV was used for Cu(I) in both oxide[100] and delafossite[101] materials, providing close agreement to experiment for structural and electronic data. However, it should be noted that at large volumes, greater than $\sim$122 Å^3, a U value of 7 eV still predicts the Ag(II)O structure as being the lowest in energy. The HSE06

simulations, on the other hand, show the correct prediction of the Ag(I,III) structure as the minimum in energy at all modeled volumes.

To allow comparison between the different methods, the predicted structural parameters for the minimum energy Ag(I,III)O and Ag(II)O structures are given for U values of 5 and 6 eV, alongside those determined with GGA and HSE06, in Table III. The GGA $+ U$ Ag(II)O structures are similar to that seen for the GGA calculation, albeit with a slightly reduced volume. For the mixed valence Ag(I,III)O structure, although GGA $+ U$ predicts a similar volume to the HSE06 calculation, the monoclinic cell is considerably more distorted in the a and b lattice vectors. In addition, the Ag(I)-O bond lengths are significantly overestimated. This increased distortion and longer bond lengths may be a consequence of applying the same U value to the $4d$ states, regardless of the silver valence state and coordination environment, rather than using different values for Ag(I) and Ag(III) species. Wang *et al.* have previously shown that different U values should be applied to different oxidation states for a range of $3d$ oxide materials.[102] However, a more extensive assessment of the application of GGA $+ U$ to the AgO system would be required to clarify this.

The calculated band structures using the GGA and HSE06 methods are detailed in Fig. 10. The GGA band structure shown is that for the Ag(I,III)O structure, despite it not being predicted as the lowest in energy, and erroneously is predicted to be semimetallic. For the HSE06-determined band structure, the VBM is found at the Γ point, whereas the CBM is present along the line from Γ-D, giving an indirect fundamental band gap of 1.0 eV. The smallest observable direct band gap has a value of 1.2 eV, which is also located along the Γ-D direction. Experimentally, an optical band gap of 1.0–1.1 eV (Refs. 103, 104) is reported, which is comparable to our theoretical direct fundamental band gap. The band structure calculated with HF (not shown) is qualitatively similar to that calculated with
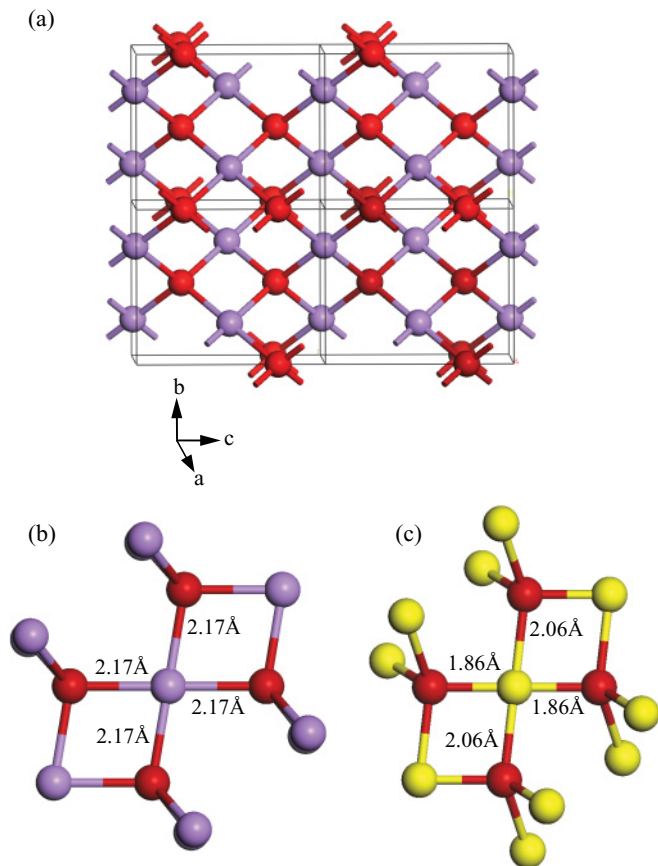
FIG. 8. (Color online) Schematic showing (a) the minimized unit cell structure of AgO as predicted using a GGA method, grown $1 \times 2 \times 2$ for clarity. Ag ions are colored purple (medium gray) and O ions are red (dark gray). The bonding environment of the silver ions, with corresponding bond lengths, is detailed in (b), while (c) shows the corresponding bonding environment in the experimental structure of Cu(II)O (Ref. 99), where copper ions are colored yellow (light gray).
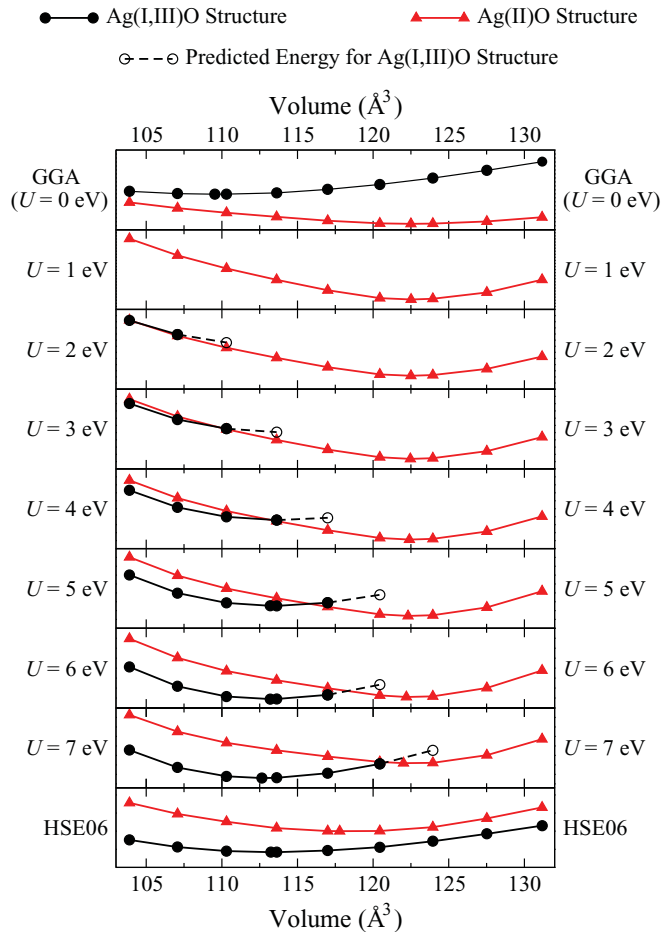

FIG. 9. (Color online) Energy-volume curves for AgO. The system was minimized as two different structures, namely, the experimental (Ref. 9) Ag(I,III)O and GGA-predicted Ag(II)O structures. These are indicated by the black (solid circles) and red (triangles) lines, respectively. Dashed lines (open circles) represent calculations where the unit-cell dimensions and shapes were held fixed as full minimization resulted in a structural change. The simulations were trialled with GGA, GGA + U (U varied from 1 to 7 eV), and HSE06 methodologies.

HSE06. However, as seen for the other oxides, the band gap is significantly overestimated. The smallest indirect and direct fundamental band gaps were found to be 9.61 and 9.62 eV, respectively.

The EDOS and PEDOS for AgO, calculated with HSE06, can be seen in Fig. 11. The VB can be represented by four regions (I–IV) and the CB by two regions (V–VI). The first region is a result of mixed O $2p$ and Ag(III) $4d$ states. Region II is seen to be a combination of $4d$ states from both Ag environments, Ag(III) s and p states and O $2p$ states. The Ag(I) $4d$ states are more dominant than those of Ag(III) though, and reach a maximum ~2.8 eV below the VBM. The VBM, region IV, consists of mixed Ag(I) $4d$ and O $2p$ states, with a small contribution from the Ag(I) $5s$. The bottom of the conduction band, region V, mainly comprises mixed Ag(III) $4d$ and O $2p$ states. Region VI is seen to contain Ag $5s$ and p states.

The PEDOSs of the Ag(I) and Ag(III) in AgO have a number of similarities to those calculated for Ag$_2$O and Ag$_2$O$_3$, respectively. The $4d$ peaks in AgO are seen to be broader in comparison to their counterparts in the single-valence binary oxides though, suggestive of a stronger interaction between Ag and O species in the mixed-valence system. The Ag(I) ions in

regions II–IV of the AgO PEDOS show a very similar structure to regions II–IV of the Ag$_2$O PEDOS (Fig. 3), particularly with the VBM comprising mixed Ag $4d$, Ag $5s$, and O $2p$ states.

For Ag$_2$O$_3$, region I of the Ag(III) and O PEDOS for AgO is similar in structure to a combination of regions I and II in the Ag$_2$O$_3$ PEDOS (Fig. 6). The top of the valence band (region III) for Ag$_2$O$_3$ shares similar features and composition to region III in the AgO PEDOS, being made up of a mix of Ag(III) s and p and O $2p$ states. The distinct CBM structure is also very similar between AgO and Ag$_2$O$_3$, possessing the unoccupied $4d$ states mixed with O $2p$ states.

D. Optical properties

The calculated optical absorption spectra for the three materials, using HSE06, is shown in Fig. 12. According to the Tauc relation:

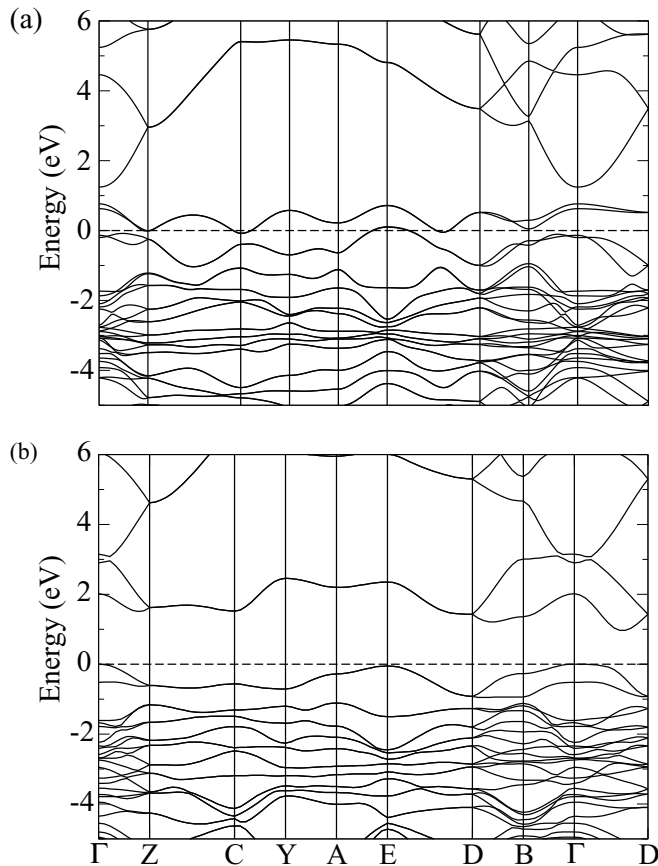$$\alpha h \nu = \text{const}(h\nu - E_g)^n, \qquad (1)$$

FIG. 10. Calculated band structure for AgO using the (a) GGA and (b) HSE06 functional. The top of the valence band in set to 0 eV, or, for GGA, the Fermi energy.

FIG. 11. (Color online) HSE06-calculated electronic density of states for AgO. (a) Total EDOS, (b) Ag(I) $5s$ and $5p$ PEDOS, (c) Ag(I) $4d$ PEDOS, (d) Ag(III) $5s$ and $5p$ PEDOS, (e) Ag(III) $4d$ PEDOS, and (f) O PEDOS. The s, p, and d states are colored blue (dashed-dotted), red (dashed), and green (solid), respectively. The Fermi energy is represented by the vertical solid gray line, which has been set to 0 eV.

where α is the absorption coefficient, $h\nu$ is the photon energy, E_g is the optical gap, and n is an index which depends on the nature of the electronic transition responsible for the absorption ($1/2$ for an allowed direct transition). Therefore, the optical band gap can be obtained from a plot of $(\alpha h\nu)^2$ vs $h\nu$ by extrapolating $(\alpha h\nu)^2$ to zero.[105–107]

For both AgO and Ag_2O_3, the onset of optical absorption is seen to correspond to transitions from the VBM to CBM at the location of the direct fundamental band gaps. For AgO, this onset occurs along the Γ-D high-symmetry line, with a calculated optical band gap of 1.40 eV. This compares reasonably well with the experimental value of 1.0–1.1 eV.[103,104] For Ag_2O_3, the onset of optical absorption occurs along the Z-L high-symmetry line and the calculated optical band gap is 2.13 eV.

For Ag_2O, the calculated optical band gap of 2.15 eV does not correspond to the fundamental band gap of 1.1 eV. This is due to transitions at the Γ point being symmetry disallowed, as is also seen for isostructural Cu_2O.[108] Instead, the onset of optical absorption is seen to occur through transitions between the top of the VB and bottom of the CB away from Γ, in both the X and M directions. The calculated optical band gap also compares favorably with the experiment of Varkey and Fort,[40] which reported a value of 2.25 eV.

Contrary to the work of Varkey and Fort, a recent study by Lyu *et al.*[41] on nanoparticles has reported an optical band gap
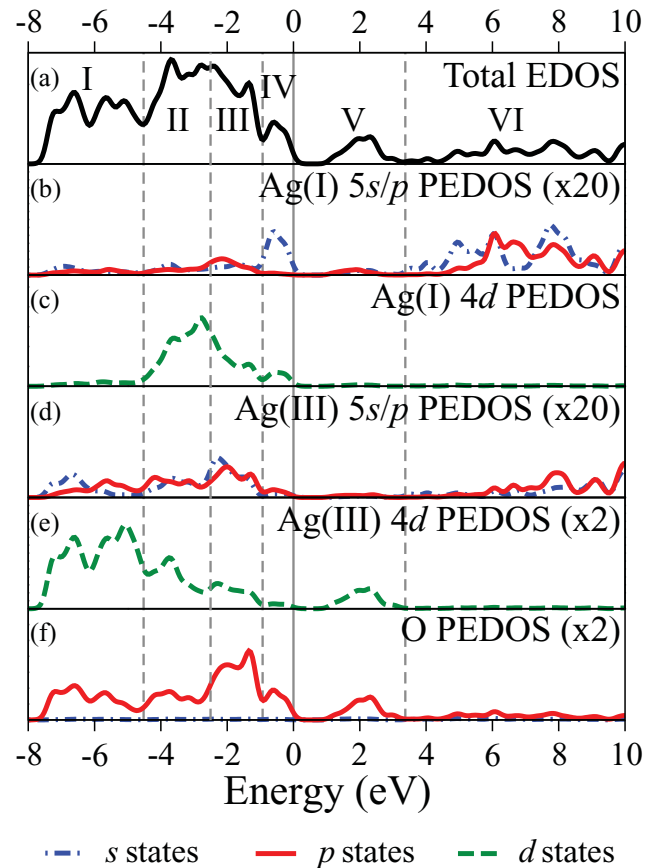
of 1.46 eV, which is also in disagreement with our calculated value. As quantum confinement has been shown to affect the size of band gaps[109] though, this questions whether the optical absorption of nanoparticles is representative of the bulk material. An optical band gap of 1.46 eV was also reported by Ida *et al.*[42] based on the study of electrodeposited Ag_2O films. However, caution should be taken with data from electrodeposited films, for example, questionable n-type conductivity was reported for the isostructural Cu_2O.[110–114] Experimental[115] and computational[67] studies have since suggested that the origin of this behavior is through the formation of an uncharacterized inversion layer on the surface of the film, which may possess some Cu(II) character. Although the formation of Ag(II) is unlikely for Ag_2O, this does raise concern over the exact stoichiometry, surface structure, and the resultant properties of thin films made through electrode-position. Furthermore, Wei *et al.* have recently reported the presence of ordered silver vacancies in electrodeposited Ag_xO nanostructures, although they made no measure of optical absorption.[116]

The calculated optical band gap of AgO, 1.40 eV, is much closer to those reported by Lyu *et al.* and Ida *et al.* Although this close agreement may simply be fortuitous, it could also suggest
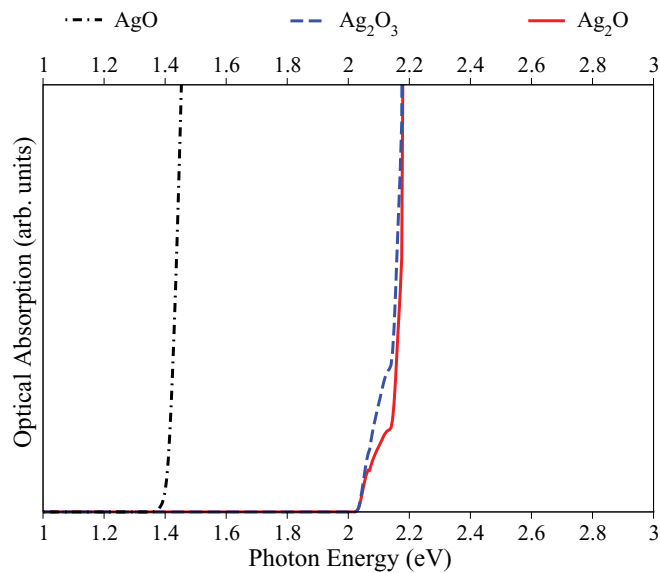
FIG. 12. (Color online) HSE06-calculated absorption spectra $(\alpha h\nu)^2$ for AgO (black/dashed-dotted), Ag_2O_3 (blue/dashed), and Ag_2O (red/solid).

that the reported absorption does not originate from pure Ag_2O. Although further investigation is needed to fully address this discrepancy, it may result from some AgO impurities or silver-deficient Ag_2O.

IV. DISCUSSION OF CRYSTAL STRUCTURES

For the silver oxides studied here, all three methods show deviations to experiment in the structural parameters. The deviations for the HF calculations are seen to differ substantially for each of the oxides. In Ag_2O, the lattice vectors are seen to be overestimated by 5.9%. However, for Ag_2O_3, this large expansion is not seen, with lattice vectors being within 1.6% of experiment and Ag(III)-O bond lengths being slightly underestimated. For AgO, a mixed situation is seen, with the unit cell distorted so that the b vector is 5.8% larger than experiment but the error in the c vector is only 0.5%. The Ag(I)-O lengths are found to be 6.9% too large, whereas the Ag(III)-O bonds are on average 2.0% too small, which is the cause of the distortion in the unit cell. Aprà *et al.* previously used HF to model AgCl and found the lattice parameter to be overestimated by 7%,[117] which corresponds with that seen in this study for Ag(I) species. This overexpansion was attributed to interionic correlation effects present in Ag(I) which are neglected by HF. To further test the importance of correlation, we simulated the Ag_2O cell with 100% HF exchange and 100% PBE correlation, finding a lattice vector only 1.2% larger than experiment. Although the physical meaning of such a calculation is questionable, it does at least indicate that the overexpansions seen for Ag(I) species with HF are a result of the neglect of correlation.

The errors in the structural parameters, relative to experiment, for both GGA and HSE06 are also larger than typically seen, although not to the extreme seen for Ag(I) species with HF. HSE06 is seen to offer only limited improvement over GGA for the calculation of the unit-cell structure (in the case of Ag_2O) or to only give substantial improvement to

some lattice vectors (Ag_2O_3 and AgO). Although the source of this is not apparent, many studies have discussed the possibility and role of Ag-Ag interactions.[37,38,118–120] DFT (and hybrid-DFT) methods are known to fail to account for nonbonded van der Waals forces,[121–123] as has been shown previously in the expansion of layered materials which are held together by dispersion forces, such as SnO (Refs. [124,125]) and V_2O_5.[72,126] To begin to assess this, we have considered the effect of dispersion corrections through the application of the GGA-D2 methodology of Grimme,[127–129] which adds dispersion corrections to the energy using a semiempirical pairwise force field. As the HSE06 approach is considerably more expensive than GGA, we initially trialled this only with the GGA approach.

The calculated lattice vectors for Ag_2O_3 and Ag_2O using GGA and GGA-D2 are given in Table IV. For Ag_2O_3, the inclusion of dispersion corrections has a large effect. Not only does it reduce all three vectors, making them closer to the experimental values, but it also equalizes the difference to experiment in all three vectors. In the original GGA calculation, the c vector was seen to have a greater error with respect to experiment than the a and b vectors. From the structure, the c vector looks to be more strongly influenced by Ag-Ag interactions. As the GGA-D2 method removes this overexpansion, it is highly suggestive of the importance of these nonbonded interactions in the silver-oxygen system. For Ag_2O, the GGA-D2 method also decreases the percentage difference in the lattice vectors relative to experiment. However, due to its cubic nature, meaning that any applied correction will inherently reduce the cell volume, no information on the appropriateness of this method can be gained.

For AgO (Table IV), the effect of dispersion corrections is not as conclusive. Although a marked improvement is seen in the a and b vectors, the c vector actually lengthens, relative to the GGA + U calculation (where $U = 6$ eV), taking it further from the experimental value. Furthermore, the potential error from using the same U value for both Ag(I) and Ag(III) species, as mentioned previously, cannot be decoupled from the effect of the dispersion interactions. However, an overall improvement is seen in the cell, suggesting that dispersion forces are also important for this structure.

Although the predicted structures are closer to those reported experimentally, an average error to experiment of 1.5% is still seen, which is more in line with typical PBE errors. In addition, the improvement seen for Ag_2O/Ag_2O_3 differs from that for AgO. The varying success of the GGA-D2 approach most likely results from the parameter set it employs. The parameters used to determine the energy corrections are based on neutral species and the van der Waals radii for the atoms. The use of atomic-based parameters puts large dispersion coefficients on the Ag atoms and small forces on the oxygen atoms. This results in the interactions between Ag atoms being too strong and those between oxygen atoms being underestimated. Furthermore, the same parameters are employed for all silver atoms, regardless of their oxidation state, which will generate additional errors for the mixed-valence system than the single-valence materials, as the results show. This is due to the different polarizabilities of Ag(I) and

TABLE IV. Calculated lattice vectors using GGA/GGA + U and GGA-D2/GGA + U-D2 methods for Ag_2O and Ag_2O_3/AgO, where $U =$ 6 eV. Percentage changes to experiment (Refs. [5],[7], and [9]) are given in parentheses and all values are in Å.

Property	Ag_2O		Ag_2O_3		AgO	
	GGA	GGA-D2	GGA	GGA-D2	GGA + U	GGA + U-D2
a	4.844 (2.4)	4.804 (1.5)	13.096 (1.8)	13.067 (1.5)	4.804 (-2.2)	5.773 (-1.5)
b	4.844 (2.4)	4.804 (1.5)	10.697 (2.0)	10.652 (1.5)	4.510 (5.2)	3.523 (1.1)
c	4.844 (2.4)	4.804 (1.5)	3.834 (4.6)	3.720 (1.5)	5.562 (1.1)	5.616 (2.1)

Ag(III) being modeled as identical. Despite these limitations, these preliminary results show that van der Waals corrections do offer a significant improvement for these materials. As the DFT-D2 methodology is unable to distinguish between the two oxidation states of Ag, we have elected not to continue trialling this approach with HSE06 and HF.

Other studies have also criticized the parameter set used in the DFT-D2 approach, notably those of Conesa[130] and Martinez-Casado *et al.*[131] Conesa assessed the use of DFT-D2 for modeling the energies of different polymorphs of TiO_2 and Al_2O_3. One of the conclusions from his work is that dispersion coefficients for neutral species should not be used and parameters determined from ionic species are more appropriate, giving a better fit to experiment. Martinez-Casado *et al.* used a range of DFT and hybrid-DFT functionals to model the adsorption of a He atom on the MgO (100) surface. Their results showed that while the application of this approach qualitatively described the correct binding of He, it failed to determine the correct binding energy, predicting an overbinding. The DFT-D2 has also been found to incorrectly model the structure of SnO, with an approach using an ionic-based parameter set offering superior structural data.[132] Alternative methods of modeling materials in which dispersion forces are important also exist and may offer improvement over the DFT-D2 method.[122] These include, but are not limited to, the nonlocal van der Waals density functional (vdw-DF)[133,134] and the improved DFT-D3 method.[135]

V. CONCLUSIONS

The results of this paper clearly show the deficiency of GGA for modeling the electronic structure of silver oxides. For Ag_2O, although GGA is able to correctly predict the general features of the band structures, in terms of their energy variation along the high-symmetry lines, it incorrectly shows it to be metallic. HSE06, however, gives a fundamental band gap of 1.2 eV, which is is good agreement with the experimental value of 1.3 eV.[35] GGA is also seen to underestimate the band gap for Ag_2O_3 by 1.4 eV, in comparison with the HSE06 results (1.9 eV). For AgO, the failure of GGA is even more dramatic, delocalizing the charge to give equivalent Ag(II) ions rather than the correct Ag(I,III) mixed valence. This is improved using a GGA + U methodology, where a U value larger than 5.0 eV is required to predict the true mixed-valence

nature of this material. HSE06 not only gives improved structural data, but is also essential for obtaining a band gap in line with experiment. HF, however, fails to predict either the structure or band gaps correctly for all three oxides. Structural data arising from Ag(I) species is seen to be overestimated in comparison to experiment, whereas Ag(III)-O bond lengths are slightly underestimated. Furthermore, band gaps predicted using HF are substantially too large, as expected for this approach.

The calculated band structures of AgO and Ag_2O_3 indicate that the fundamental band gaps are indirect in nature, 1.0 and 1.9 eV, respectively. The smallest direct band gaps, however, are only slightly larger in energy and are also the location of the optical band gaps (1.40 and 2.13 eV), respectively. Ag_2O differs with these oxides in that it has a direct fundamental band gap of 1.1 eV which is symmetry forbidden. Therefore, the optical band gap is larger, with a calculated value of 2.15 eV. This calls into question recent experimental optical band gaps from Ag_2O nanoparticles and electrodeposited thin films of 1.46 eV. The close agreement of this with our calculated optical band gap of AgO suggests that the experimental value may not originate from pure Ag_2O, but possibly from AgO impurities or silver-deficient Ag_2O. This indicates the need for further study to clarify this discrepancy.

Finally, preliminary calculations have been conducted to consider the importance of nonbonded van der Waals interactions for the silver-oxygen system. The GGA-D2 method of Grimme highlights that the inclusion of dispersion corrections can significantly improve the structural prediction of these oxides, suggesting that these corrections are important. However, the atomic parameters derived for neutral species used in this method may not be appropriate for use with these oxides, which possess silver ions with different oxidation states. This is particularly true for AgO, for which a distorted unit cell is still predicted with GGA + U-D2.

*allenje@tcd.ie

†watsong@tcd.ie

[1] P. Niggli, Z. Kristallogr. **57**, 253 (1922).

[2] M. O'Keeffe and J. O. Bovin, Am. Mineral. **63**, 180 (1978).

[3] P. Jones, H. Rumpel, E. Schwarzmann, G. Sheldrick, and H. Paulus, Acta Crystallogr. Sect. B **35**, 1435 (1979).

[4] J. J. Pireaux, M. Liehr, P. A. Thiry, J. P. Delrue, and R. Caudano, Surf. Sci. **141**, 221 (1984).

[5] P. Norby, R. Dinnebier, and A. N. Fitch, Inorg. Chem. **41**, 3628 (2002).

[6] B. Standke and M. Jansen, Angew. Chem. **97**, 114 (1985).

[7] B. Standke and M. Jansen, Angew. Chem., Int. Ed. Engl. **24**, 118 (1985).

[8] B. Standke and M. Jansen, Z. Anorg. Allg. Chem. **535**, 39 (1986).

[9] M. Jansen and P. Fischer, J. Less-Common Met. **137**, 123 (1988).

[10] B. Standke and M. Jansen, Angew. Chem. **98**, 78 (1986).

[11] B. Standke and M. Jansen, Angew. Chem., Int. Ed. Engl. **25**, 77 (1986).

[12] B. Standke and M. Jansen, J. Solid State Chem. **67**, 278 (1987).

[13] G. I. N. Waterhouse, J. B. Metson, and G. A. Bowmaker, Polyhedron **26**, 3310 (2007).

[14] A. N. Mansour, J. Phys. Chem. **94**, 1006 (1990).

[15] W. Beesk, P. G. Jones, H. Rumpel, E. Schwarzmann, and G. M. Sheldrick, J. Chem. Soc. Chem. Commun. **14**, 664 (1981).

[16] D. F. Smith and J. A. Gucinski, J. Power Sources **80**, 66 (1999).

[17] D. F. Smith and C. Brown, J. Power Sources **96**, 121 (2001).

[18] J. Pan, Y. Sun, Z. Wang, P. Wan, X. Liu, and M. Fan, J. Mater. Chem. **17**, 4820 (2007).

[19] H. Q. Li, Y. G. Wang, P. He, and H. S. Zhou, Chem. Commun. **46**, 2055 (2010).

[20] D. Dellasega, A. Facibeni, F. Di Fonzo, M. Bogana, A. Polissi, C. Conti, C. Ducati, C. S. Casari, A. Li Bassi, and C. E. Bottani, Nanotechnology **19**, 475602 (2008).

[21] D. Dellasega, A. Facibeni, F. Di Fonzo, V. Russo, C. Conti, C. Ducati, C. S. Casari, A. Li Bassi, and C. E. Bottani, Appl. Surf. Sci. **255**, 5248 (2009).

[22] X. Wang, H. F. Wu, Q. Kuang, R. B. Huang, Z. X. Xie, and L. S. Zheng, Langmuir **26**, 2774 (2010).

[23] J. Tominaga, J. Phys. Condens. Matter **15**, R1101 (2003).

[24] B. Fang, A. Gu, G. Wang, W. Wang, Y. Feng, C. Zhang, and X. Zhang, ACS Appl. Mater. Interfaces **1**, 2829 (2009).

[25] W. Wang, Q. Zhao, J. Dong, and J. Li, Int. J. Hydrogen Energy **36**, 7374 (2011).

[26] M. Fujimaki, K. Awazu, and J. Tominaga, J. Appl. Phys. **100**, 074303 (2006).

[27] R. H. Crabtree, J. Organomet. Chem. **690**, 5451 (2005).

[28] Q. Y. Tian, D. X. Shi, and Y. W. Sha, Molecules **13**, 948 (2008).

[29] C. Tomasi, P. Mustarelli, and A. Magistris, J. Solid State Chem. **140**, 91 (1998).

[30] M. Hosono, J. Kawamura, I. H., N. Kuwata, T. Kamiyama, and Y. Nakamura, J. Non-Cryst. Solids **244**, 81 (1999).

[31] H. Takahashi, N. Rikitake, T. Sakuma, and Y. Ishii, Solid State Ionics **168**, 93 (2004).

[32] Z. Wiśniewski, R. Wiśniewski, and J. L. Nowiński, Solid State Ionics **157**, 275 (2003).

[33] A. Deb and A. K. Chatterjee, J. Phys. Condens. Matter **10**, 11719 (1998).

[34] M. T. Czyżyk, R. A. de Groot, G. Dalba, P. Fornasini, A. Kisiel, F. Rocca, and E. Burattini, Phys. Rev. B **39**, 9831 (1989).

[35] L. H. Tjeng, M. B. J. Meinders, J. van Elp, J. Ghijsen, and G. A. Sawatzky, Phys. Rev. B **41**, 3190 (1990).

[36] G. B. Hoflund, Z. F. Hazos, and G. N. Salaita, Phys. Rev. B **62**, 11126 (2000).

[37] A. Filippetti and V. Fiorentini, Phys. Rev. B **72**, 035128 (2005).

[38] A. B. Gordienko, Y. N. Zhuravlev, and D. G. Fedorov, Phys. Solid State **49**, 223 (2007).

[39] F. Pei, S. Wu, G. Wang, M. Xu, S.-Y. Wang, and L.-Y. Chen, J. Korean Phys. Soc. **55**, 1243 (2009).

[40] A. J. Varkey and A. F. Fort, Sol. Energy Mater. Sol. Cells **29**, 253 (1993).

[41] L.-M. Lyu, W.-C. Wang, and M. H. Huang, Chem. Eur. J. **16**, 14167 (2010).

[42] Y. Ida, S. Watase, T. Shinagawa, M. Watanabe, M. Chigane, M. Inaba, A. Tasaka, and M. Izaki, Chem. Mater. **20**, 1254 (2008).

[43] P. Behrens, S. Aßmann, U. Bilow, C. Linke, and M. Jansen, Z. Anorg. Allg. Chem. **625**, 111 (1999).

[44] L. van Wüllen, S. Vensky, W. Hoffbauer, and M. Jansen, Solid State Sci. **7**, 920 (2005).

[45] J. K. Burdett and S. Sevov, J. Am. Chem. Soc. **117**, 12788 (1995).

[46] D. Lützenkirchen-Hecht and H.-H. Strehblow, Surf. Interface Anal. **41**, 820 (2009).

[47] M. Bielmann, P. Schwaller, P. Ruffieux, O. Gröning, L. Schlapbach, and P. Gröning, Phys. Rev. B **65**, 235431 (2002).

[48] K.-T. Park, D. L. Novikov, V. A. Gubanov, and A. J. Freeman, Phys. Rev. B **49**, 4425 (1994).

[49] J. P. Allen, D. O. Scanlon, and G. W. Watson, Phys. Rev. B **81**, 161103 (2010).

[50] G. Kresse and J. Hafner, Phys. Rev. B **49**, 14251 (1994).

[51] G. Kresse and J. Furthmüller, Phys. Rev. B **54**, 11169 (1996).

[52] P. E. Blöchl, Phys. Rev. B **50**, 17953 (1994).

[53] G. Kresse and D. Joubert, Phys. Rev. B **59**, 1758 (1999).

[54] J. P. Perdew, K. Burke, and M. Ernzerhof, Phys. Rev. Lett. **77**, 3865 (1996).

[55] S. Heyd, G. E. Scuseria, and M. Ernzerhof, J. Chem. Phys. **118**, 8207 (2003).

[56] A. V. Krukau, O. A. Vydrov, A. F. Izmaylov, and G. E. Scuseria, J. Chem. Phys. **125**, 224106 (2006).

[57] D. O. Scanlon, A. Walsh, and G. W. Watson, Chem Mater. **21**, 4568 (2009).

[58] J. Heyd and G. E. Scuseria, J. Chem. Phys. **121**, 1187 (2004).

[59] J. Heyd, J. E. Peralta, G. E. Scuseria, and R. L. Martin, J. Chem. Phys. **123**, 174101 (2005).

[60] M. Marsman, J. Paier, A. Stroppa, and G. Kresse, J. Phys. Condens. Matter **20**, 064201 (2008).

[61] S. Chen, Z. G. Gong, A. Walsh, and S. H. Wei, Appl. Phys. Lett. **94**, 041903 (2009).

[62] J. Paier, R. Asahi, A. Nagoya, and G. Kresse, Phys. Rev. B **79**, 115126 (2009).

[63] D. O. Scanlon and G. W. Watson, Chem. Mater. **21**, 5435 (2009).

[64] D. O. Scanlon and G. W. Watson, Appl. Phys. Lett. **97**, 131904 (2010).

[65] A. Stroppa and G. Kresse, Phys. Rev. B **79**, 201201(R) (2009).

[66] D. O. Scanlon and G. W. Watson, J. Phys. Chem. Lett. **1**, 3195 (2010).

[67] D. O. Scanlon and G. W. Watson, J. Phys. Chem. Lett. **1**, 2582 (2010).

[68] I. D. Prodan, G. E. Scuseria, and R. L. Martin, Phys. Rev. B **73**, 045104 (2006).

[69] J. L. F. Da Silva, M. V. Ganduglia-Pirovano, J. Sauer, V. Bayer, and G. Kresse, Phys. Rev. B **75**, 045121 (2007).

[70] A. Stroppa and S. Picozzi, Phys. Chem. Chem. Phys. **12**, 5405 (2010).

[71] E. N. Brothers, A. F. Izmaylov, J. O. Normand, V. Barone, and G. E. Scuseria, J. Chem. Phys. **129**, 011102 (2008).

[72] D. O. Scanlon, A. Walsh, B. J. Morgan, and G. W. Watson, J. Phys. Chem. C **112**, 9903 (2008).

[73] D. O. Scanlon, N. M. Galea, B. J. Morgan, and G. W. Watson, J. Phys. Chem. C **113**, 11095 (2009).

[74] R. Coquet and D. J. Willock, Phys. Chem. Chem. Phys. **7**, 3819 (2005).

[75] P. R. L. Keating, D. O. Scanlon, and G. W. Watson, J. Phys. Condens. Matter **21**, 405502 (2009).

[76] B. J. Morgan, D. O. Scanlon, and G. W. Watson, J. Mater. Chem. **19**, 5175 (2009).

[77] D. O. Scanlon, A. Walsh, B. J. Morgan, M. Nolan, J. Fearon, and G. W. Watson, J. Phys. Chem. C **111**, 7971 (2007).

[78] M. Nolan and G. W. Watson, J. Chem. Phys. **125**, 144701 (2006).

[79] S. L. Dudarev, G. A. Botton, S. Y. Savrasov, C. J. Humphreys, and A. P. Sutton, Phys. Rev. B **57**, 1505 (1998).

[80] F. D. Murnaghan, Proc. Natl. Acad. Sci. USA **30**, 244 (1944).

[81] M. Gajdos, K. Hummer, G. Kresse, J. Furthmüller, and F. Bechstedt, Phys. Rev. B **73**, 045112 (2006).

[82] B. Adolph, J. Furthmüller, and F. Beckstedt, Phys. Rev. B **63**, 125108 (2001).

[83] L. E. Ramos, J. Paier, G. Kresse, and F. Bechstedt, Phys. Rev. B **78**, 195423 (2008).

[84] J. Paier, M. Marsman, and G. Kresse, Phys. Rev. B **78**, 121201 (2008).

[85] X. Nie, S. H. Wei, and S. B. Zhang, Phys. Rev. Lett. **88**, 066405 (2002).

[86] A. Walsh, J. L. F. Da Silva, Y. Yan, M. M. Al-Jassim, and S. H. Wei, Phys. Rev. B **79**, 073105 (2009).

[87] A. Walsh, Y. Yan, M. N. Huda, M. M. Al-Jassim, and S. H. Wei, Chem. Mater. **21**, 547 (2009).

[88] A. Kirfel and K. Eichhorn, Acta Crystallogr. Sect. A **46**, 271 (1990).

[89] C. E. Housecroft and A. G. Sharpe, *Inorganic Chemistry* (Pearson Education, Harlow, UK, 2001).

[90] D. O. Scanlon and G. W. Watson, J. Mater. Chem. **21**, 3655 (2011).

[91] J. P. Allen, M. K. Nilsson, D. O. Scanlon, and G. W. Watson, Phys. Rev. B **83**, 035207 (2011).

[92] C. J. Bradley and A. P. Cracknell, *Mathematical Theory of Symmetry in Solids* (Oxford University Press, Oxford, UK, 1972).

[93] D. O. Scanlon, B. J. Morgan, G. W. Watson, and A. Walsh, Phys. Rev. Lett. **103**, 096405 (2009).

[94] D. O. Scanlon and G. W. Watson, Phys. Chem. Chem. Phys. **13**, 9667 (2011).

[95] N. Umezawa, O. Shuxin, and J. Ye, Phys. Rev. B **83**, 035202 (2011).

[96] R. Restori and D. Schwarzenbach, Acta Crystallogr. Sect. B **42**, 201 (1986).

[97] H. Shi, R. Asahi, and C. Stampfl, Phys. Rev. B **75**, 205125 (2007).

[98] K. Yvon, A. Bezinge, P. Tissot, and P. Fischer, J. Solid State Chem. **65**, 225 (1986).

[99] A. Stergiou, I. Kerasiotis, and C. Stergiou, J. Optoelectron. Adv. Mater. **9**, 1772 (2007).

[100] D. O. Scanlon, B. J. Morgan, and G. W. Watson, J. Chem. Phys. **131**, 124703 (2009).

[101] D. O. Scanlon, A. Walsh, B. J. Morgan, G. W. Watson, D. J. Payne, and R. G. Egdell, Phys. Rev. B **79**, 035101 (2009).

[102] L. Wang, T. Maxisch, and G. Ceder, Phys. Rev. B **73**, 195107 (2006).

[103] B. E. Breyfogle, C. J. Hung, M. G. Shumsky, and J. A. Switzer, J. Electrochem. Soc. **143**, 2714 (1996).

[104] N. Ravi Chandra Raju, K. Jagadeesh Kumar, and A. Subrahmanyam, J. Phys. D **42**, 135411 (2009).

[105] M. Beaudoin, M. Meunier, and C. J. Arenault, Phys. Rev. B **47**, 2197 (1993).

[106] G. P. Joshi, N. S. Saxena, R. Mangal, A. Mishra, and T. P. Sharma, Bull. Mater. Sci. **26**, 387 (2003).

[107] N. J. Tharayil, R. Raveendran, A. V. Vaidyan, and P. G. Chithra, Indian J. Eng. Mater. Sci. **15**, 489 (2008).

[108] J. P. Dahl and A. C. Switendick, J. Phys. Chem. Solids **27**, 931 (1966).

[109] H.-X. Deng, S.-S. Li, and J. Li, J. Phys. Chem. C **114**, 4841 (2010).

[110] W. Siripala and J. R. P. Jaykody, Sol. Energy Mater. **14**, 23 (1986).

[111] C. Jayewardena, K. P. Hewaparakrama, D. L. A. Wijewardena, and H. Guruge, Sol. Energy Mater. Sol. Cells **56**, 29 (1998).

[112] C. A. N. Fernando and S. K. Wetthasinghe, Sol. Energy Mater. Sol. Cells **63**, 299 (2000).

[113] R. Garuthara and W. Siripala, J. Lumin. **121**, 173 (2006).

[114] L. C. Wang and M. Tao, Electrochem. Solid-State Lett. **10**, H248 (2007).

[115] J. N. Nian, C. C. Tsai, P. C. Lin, and H. S. Teng, J. Electrochem. Soc. **156**, H567 (2009).

[116] W. Wei, X. Mao, L. A. Ortiz, and D. R. Sadoway, J. Mater. Chem. **21**, 432 (2011).

[117] E. Aprà, E. Stefanovich, R. Dovesi, and C. Roetti, Chem. Phys. Lett. **186**, 329 (1991).

[118] P. Pyykkö, Chem. Rev. **97**, 597 (1997).

[119] E. Ruiz, S. Alvarez, A. Alemany, and R. Evarestov, Phys. Rev. B **56**, 7189 (1997).

[120] S. Sculfort, P. Croizat, A. Messaoudi, M. Bénard, M.-M. Rohmer, R. Welter, and P. Braunstein, Angew. Chem. Int. Ed. **48**, 9663 (2009).

[121] W. Koch, E. Jan Baerends, and M. C. Holthausen, *A Chemist's Guide to Density Functional Theory* (Wiley-VCH, Weinheim, 2001).

[122] J. F. Dobson, K. McLennan, A. Rubio, J. Wang, T. Gould, H. M. Le, and B. P. Dinte, Aust. J. Chem. **54**, 513 (2001).

[123] Q. Wu and W. Yang, J. Chem. Phys. **116**, 515 (2002).

[124] G. W. Watson, J. Chem. Phys. **114**, 758 (2001).

[125] A. Walsh and G. W. Watson, Phys. Rev. B **70**, 235114 (2004).

[126] E. Londero and E. Schröder, Phys. Rev. B **82**, 054116 (2010).

[127] S. Grimme, J. Comput. Chem. **25**, 1463 (2004).

[128] S. Grimme, J. Comput. Chem. **27**, 1787 (2006).

[129] T. Bučko, J. Hafner, S. Lebègue, and J. G. Ángyán, J. Phys. Chem. A **114**, 11814 (2010).

[130]J. C. Conesa, J. Phys. Chem. C **114**, 22718 (2010).

[131]R. Martinez-Casado, G. Mallia, D. Usvyat, L. Maschio, S. Casassa, M. Schütz, and N. M. Harrison, J. Chem. Phys. **134**, 014706 (2011).

[132]J. P. Allen, D. O. Scanlon, S. C. Parker, and G. W. Watson, J. Phys. Chem. C (2011), doi: 10.1021/jp205148y.

[133]M. Dion, H. Ryberg, E. Schröder, D. C. Langreth, and B. I. Lundqvist, Phys. Rev. Lett. **92**, 246401 (2004).

[134]J. Klimeš, D. R. Bowler, and A. Michaelides, J. Phys. Condens. Matter **22**, 022201 (2010).

[135]S. Grimme, J. Antony, S. Ehrlich, and H. Krieg, J. Chem. Phys. **132**, 154104 (2010).